RSC Advances

PAPER

View Article Online
View Journal | View Issue

Cite this: *RSC Adv.*, 2018, **8**, 17300

Modification of Talc@TiO_2 toward high-performance nitrile rubber application

Chao He,[a] Lin Zhang,[a] Duoli Chen,[a] Xiaoqiang Fan,*[a] Zhenbing Cai[b] and Minhao Zhu*[ab]

Received 4th February 2018
Accepted 24th April 2018

DOI: 10.1039/c8ra01091a

rsc.li/rsc-advances

To improve the dispersion of talcum powder (Talc) for polymer applications, modified nano-titania powders (TiO_2) using a silane coupling agent (KH550), a titanate coupling agent (NDZ201) and sodium polyacrylate (PAAS) were well adhered to the surface of Talc with a ball milling method, thereby preparing a series of mixed Talc@TiO_2 particles to realize good dispersion in carboxylated acrylonitrile–butadiene rubber (XNBR). Note that Talc@TiO_2 particles modified by PAAS and NDZ201 show better colloidal dispersion in anhydrous ethanol due to organification and repulsion of charge, with original Talc and NDZ201 modified Talc@TiO_2 powders as a comparison. Modified Talc@TiO_2 hybrid XNBR shows good performance characteristics, including damping capacity and impact resistance, depending mainly on the excellent mechanical property of Talc, good dispersion and the high adhesive force between modified Talc@TiO_2 and XNBR.

1. Introduction

The blending of organic/inorganic fillers with matrix materials is a common approach to tailoring their performance characteristics, because the introduction of fillers by simple and low-cost techniques can obtain the expected physicochemical and mechanical properties of matrix materials due to nature of the fillers, their size and shape, distribution and adhesion in the composite.[1–4] Primordial Talc composed primarily of hydrated magnesium silicate with a molecular formula of $3MgO{\cdot}4SiO_2{\cdot}H_2O$ has aroused wide interest in academe and industry because of its bargain price, surface paintability and high mechanical strength. Talc is often encountered as an important filler to enhance the mechanical behaviors of polymer materials,[5–8] but as a passive filler it has always found it difficult to achieve widespread application. And Talc particles are prone to aggregation because of their high surface energy. To realize Talc applications in polymers, scholars have taken action to obtain satisfactory compatibility with organic compounds, such as surface chemical modification, surface physical coating, plasma surface treatment, and mechano-chemistry to modify the surface of the inorganic particles.[9,10]

Talc hybrid polypropylene (PP) composites have been extensively prepared by reactive mixing of raw materials (including PP, Talc and improvers), the addition of inorganic and organic acid modified Talc powers as fillers, and so forth, and their physicochemical and mechanical properties have been studied in the past.[11–15] Talc powders which have been acid activated and modified by organic surfactant have also been prepared and used as fillers in rubber to improve its mechanical and damping properties.[10,16–19] Unfortunately, up to now, there has been no simple and sufficient approach to Talc surface modification and one-step modification technology has not been able to have an impact on ameliorating aggregation, improving dispersion and enhancing the interfacial adhesion between the filler and matrix materials. Recently, an organic and inorganic coordinated modification approach has attracted attention, and hybrid composites using this method have shown excellent mechanical performance *via* the synergy of organic and inorganic phases at the nano-scale or even at the molecular level.[20–23] Titania nanoparticles could perform with outstanding function, dispersing better in matrix materials than other nanoparticles.[24] The chemical formula of Talc is $3MgO{\cdot}4SiO_2{\cdot}H_2O$, so it contains the massive SiO_2. As in previous studies on silica-titania nanoparticles, TiO_2 performed with high chemical stability, high activity, non-toxicity and high photoelectric conversion efficiency when used in mixed particles.[25,26] Surfactant molecules are essential for solving the poor dispersion and compatibility of nanoparticles through repulsive interaction.[27–29] A great deal of research on diverse surfactant and modification mechanisms has been conducted,[30–33] and it has been found that coupling agents can improve the surface hydrophobicity of inorganic particles by chemical bonding, including a silane coupling agent and a titanate coupling agent. And water-soluble polymers like sodium polyacrylate (PAAS) can

[a]*Key Laboratory of Advanced Technologies of Materials (Ministry of Education), School of Materials Science and Engineering, Southwest Jiaotong University, Chengdu 610031, China. E-mail: fxq@home.swjtu.edu.cn; Fax: +86 028 87600128; Tel: +86 028 87600128*

[b]*Tribology Research Institute, State Key Laboratory of Traction Power, Southwest Jiaotong University, Chengdu 610031, China. E-mail: zhuminhao@swjtu.cn*

Table 1 Performance parameters of XNBR

Parameters	Typical value
Acrylonitrile content (%)	27
Carboxyl content (%)	7
Mooney viscosity ML_{1+4} at 100 °C	34

also sufficiently improve the dispersion of inorganic particles.[34,35]

XNBR is the product of NBR after the introduction of carboxyl groups and it is always used as a sealing material. As a class of special high-performance rubber with the carboxyl group along the chain, it has good wear resistance and excellent mechanical and damping properties. The carboxyl groups along the chain have the possibility of reacting with the OH of the fillers.[36] These reactive and polar functional groups make it a suitable candidate for exploring the interaction between the rubber matrix and the various fillers, and developing some novel composite materials.[37,38]

In this paper, a series of Talc@TiO_2 particles with good dispersion were prepared using a collaborative modification method with reactive mixing of organic modified titania nanoparticles and Talc by ball milling. A silane coupling agent (KH550), titanate coupling agent (NDZ201) and PAAS (ACUME9300) were chosen to modify the titania nanoparticles. Then Talc@TiO_2 hybrid carboxylated acrylonitrile–butadiene rubbers (XNBR) were prepared, and their mechanical behaviors were evaluated in detail.

2. Experimental section

2.1 Materials

Original Talc was obtained from the Guilin Xinhua Hui Factory of Ultrafine Powder (Guangxi, China). KH550 and NDZ201 were purchased from Dongguan City Ding Hai Plastic Chemical Co., Ltd. ACUMER9300 was commercially obtained from the DOW Chemical Company. Solid XNBR was obtained from the NANTEX Industry Co. Ltd. The performance parameters of XNBR are shown in Table 1. All of the reagents were analytical-grade.

2.2 Preparation of Talc@TiO_2 fillers and hybrid XNBR

Before modification, Talc and TiO_2 particles were dried in a vacuum oven at 60 °C for 12 h to remove the absorbed moisture on the surface. 2 g of TiO_2 nanoparticles were dispersed in a mixed solution of 90 ml of anhydrous ethanol and 30 ml of deionized water with ultrasonic dispersion for 20 min to ensure that TiO_2 was completely dispersed. 0.2 g of NDZ201, ACUMER9300 and hydrolysis treated KH550 were added, respectively. The pH value of the solutions was regulated successively at 5 and 10 at 50 °C for an hour under ultrasonic treatment. Then the products were washed by centrifugation with anhydrous ethanol and deionized water several times. The modified TiO_2 particles were obtained after drying in a vacuum oven for 12 h at 60 °C.

10 g of Talc particles were pre-ground by a ball mill for 1 h to stimulate their surface activity. 2 g of modified TiO_2 particles were added and mixed with the Talc particles in moderate

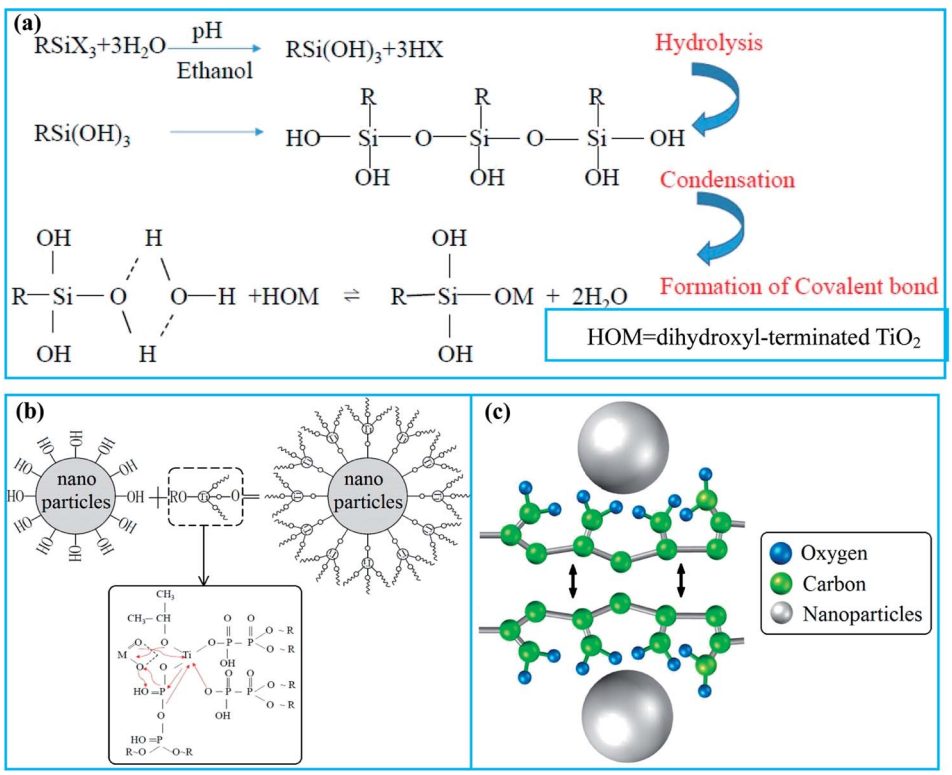

Fig. 1 Schematic illustration of organic modification of TiO_2 nanoparticles: (a) KH550-modified TiO_2, (b) NDZ201-modified TiO_2, (c) PAAS-modified TiO_2.

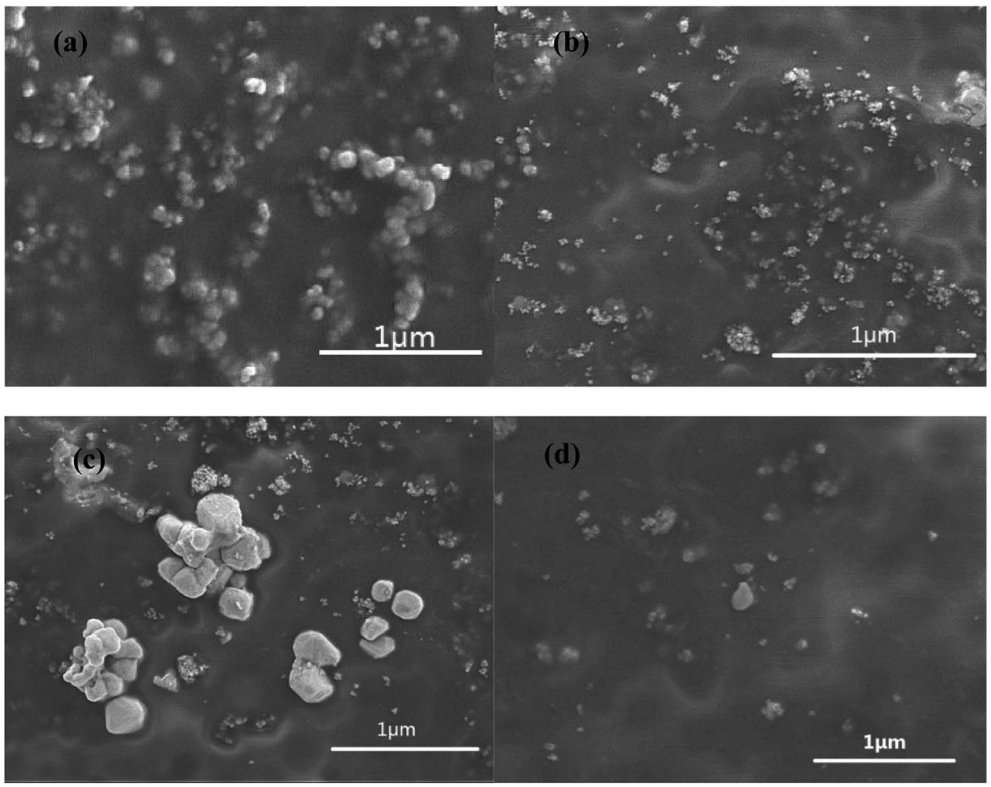

Fig. 2 SEM images of raw and modified TiO_2 particles: (a) raw TiO_2, (b) NDZ201-TiO_2, (c) KH550-TiO_2, (d) PAAS-TiO_2.

anhydrous ethanol at a constant velocity of 300 rpm for 2 h. After the mixtures were dried for 12 h at 80 °C, modified Talc@TiO_2 particles were obtained and were abbreviated to KH550-Talc@TiO_2, NDZ201-Talc@TiO_2 and PAAS-Talc@TiO_2 according to the different surfactants, with surfactant-free Talc@TiO_2 particles as a comparison. The modification of TiO_2 nanoparticles by these organic agents is schematically illustrated in Fig. 1.

XNBR was plasticated by a two-roller mill at 15 rpm for 3 min, and then the fillers were mixed with XNBR using the two-roller mill for 5 min. The mixing ratios of fillers were increased according to 5 wt%, 10 wt% and 15 wt%. Samples were mould-compressed by a press moulding machine under the following conditions: 150 °C, 15 MPa and 20 min.

These modified Talc@TiO_2 particles with a weight content of 10 wt% fillers were added into the XNBR and mixed for 10 min. Modified Talc@TiO_2 hybrid XNBR composites were obtained by compression moulding in a twin-screw extruder at 160 °C.

2.3 Characterization of modified Talc@TiO_2 fillers and hybrid XNBR

The morphology of the original and modified TiO_2 particles was investigated by a JSM-7800F field-emission scanning electron microscope (SEM) (JEOL, Japan), and the functional groups on these modified TiO_2 particles were investigated by Fourier transform infrared (FTIR) (PerkinElmer16PC, USA) in the wave number range 4000 cm^{-1} to 500 cm^{-1}.

The surface hydrophilicity of the modified Talc@TiO_2 blocks was measured by a DSA100 instrument (KRUSS, Germany) at room temperature. 1 μl of water was dropped onto the surface of the modified Talc@TiO_2 blocks and the contact angle data were recorded. The morphology of the modified Talc@TiO_2 particles was investigated by SEM (JSM-6610LV, JEOL, Japan). FTIR spectra of the modified Talc@TiO_2 particles were also obtained by a PerkinElmer 16PCFTIR spectrometer. An X-ray photoelectron spectroscope (XPS) (ESCALAB 250Xi, USA) was used to investigate the chemical states of the typical elements from the modifiers to further confirm the modification mechanism of the modified Talc@TiO_2 particles.

Sedimentation of Talc and modified Talc@TiO_2 was tested with a sedimentation pipe. An appropriate amount of Talc and modified Talc@TiO_2 were added individually to sedimentation pipes until they were evenly dispersed using ultrasonic treatment. After a certain interval of time, the mixtures were photographed to evaluate the sedimentation of the particles.

The morphology of the modified Talc@TiO_2 hybrid XNBR was investigated by JSM-6610LV SEM, and their mechanical properties (including a tensile test, damping and anti-impact behaviors) were evaluated by a tensile machine (AGS-J, SHIMADZU, China), a dynamic mechanical analyzer (DMA) (Q800, USA) and a home-made impact-sliding test rig.

3. Results and discussion

3.1 Analysis of modified TiO_2 particles

To observe the morphology of three types of modified TiO_2 nanoparticles and compare them with their aggregations, Fig. 2 shows the SEM micrographs of raw and modified TiO_2 for

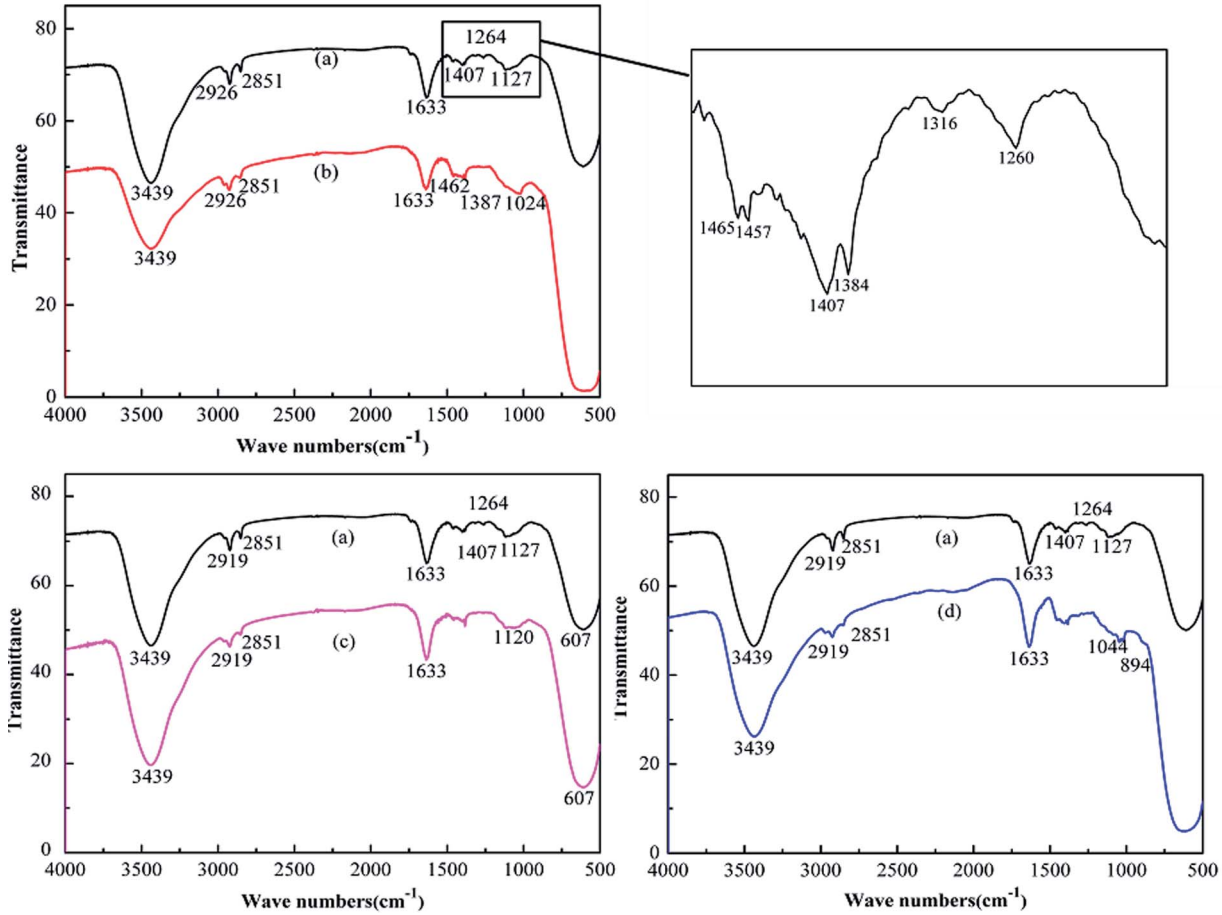

Fig. 3 FTIR spectra of modified TiO_2 particles, with raw TiO_2 as a comparison: (a) TiO_2, (b) NDZ201-TiO_2, (c) KH550-TiO_2, (d) PAAS-TiO_2.

contrast. Raw TiO_2 particles have a relatively high degree of agglomeration due to the nano-size effects with high surface energy. After being modified by coupling agents (KH550 and NDZ201), these organic molecules stick onto the surface of TiO_2 *via* physical adsorption and chemical bonding interaction to form an organic molecular layer which prevents their aggregation. The function of NDZ201 is superior to that of KH550, one possible reason being that KH550 does not completely react with TiO_2 during polycondensation in solution. PAAS with a negative charge has the function of charge mutual repulsion in a mixed solution with TiO_2 nanoparticles. PAAS is prone to transform into a gel in solution, so PAAS favors the formation of a molecular layer on the surface of the particles, suggesting that PAAS modified TiO_2 particles will show good dispersibility with low agglomeration.

Fig. 3 shows FTIR spectra of modified TiO_2 to confirm the presence of functional groups, with raw TiO_2 as a comparison. As shown in Fig. 3, organic modification reconciled some characteristic peaks in the region 1200–1500 cm^{-1}, and some other characteristic peaks disappeared after modification, including bands of NDZ201-TiO_2 at 1316 cm^{-1} and 1024 cm^{-1}, and a band of KH550-TiO_2 at 1260 cm^{-1}. After organic modification, some new characteristic peaks appeared on the spectra, such as KH550-TiO_2 with Si–O vibration absorption at 1120 cm^{-1}, and PAAS-TiO_2 with carboxyl absorption bands at 1044 cm^{-1} and 894 cm^{-1}.[39] The characteristic peak of TiO_2 at 1127 cm^{-1} moved to 1120 cm^{-1} after modification by KH550. FTIR results indicate that TiO_2 particles have been effectively modified by coupling agents and surfactant.

3.2 Analysis of modified Talc@TiO_2

The surface hydrophilicity of as-prepared Talc@TiO_2 particles was evaluated to reflect the affinity between the filler and matrix materials. The contact angle data are shown in Fig. 4. Their contact angles increase in the following sequence: Talc@TiO_2 (67.5°) < PAAS-Talc@TiO_2 (68.3°) < KH550-Talc@TiO_2 (71.5°) < NDZ201-Talc@TiO_2 (90.4°). The results illustrate that the hydrophilicity of the as-prepared particles decreases with the use of an organic modifier, especially NDZ201-Talc@TiO_2, which has become hydrophobic. This phenomenon could be attributed to the interaction between the carboxyl group of NDZ201 and the hydroxyl group absorbed on the surface of nano TiO_2, thereby achieving the purpose of chemical coupling.[40] PAAS (ACUMER9300) is a kind of water-soluble macro-molecule without a hydrophobic group and KH550 has low solubility in aqueous media which affects the condensation reaction and effective modification, so there is no substantial increase in contact angle on PAAS-Talc@TiO_2 or KH550-Talc@TiO_2. These indicate that the modified TiO_2 nano-

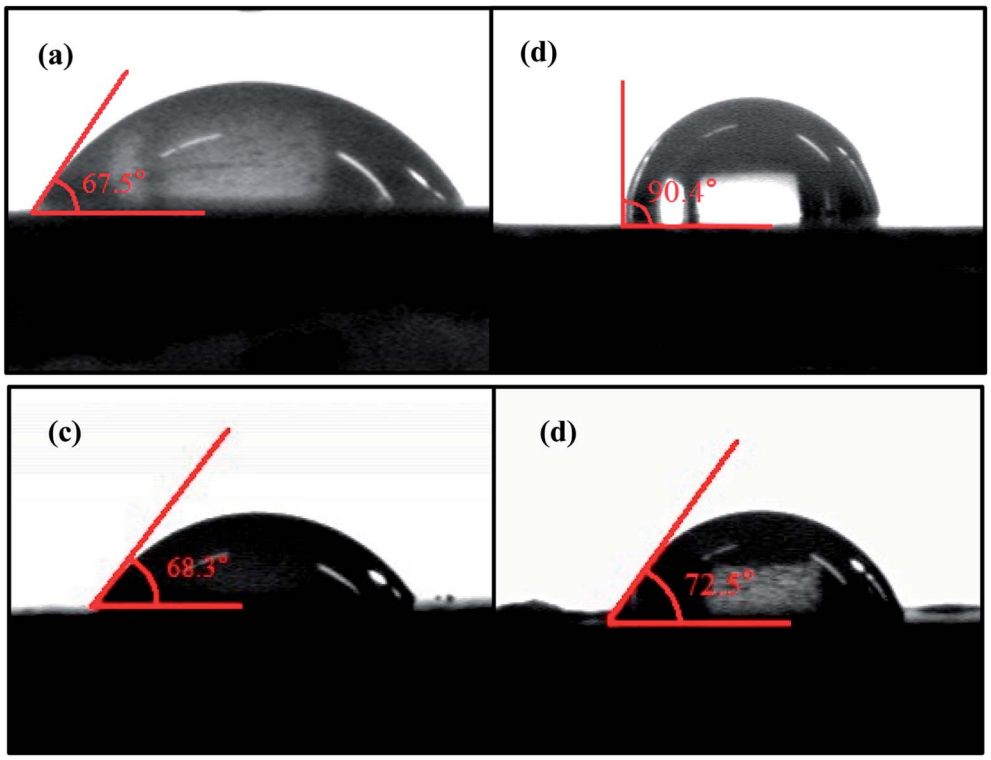

Fig. 4 Contact angle of (a) Talc@TiO_2, (b) NDZ201-Talc@TiO_2, (c) KH550-Talc@TiO_2, (d) PAAS-Talc@TiO_2.

particles were deposited or adhered on the surface of Talc particles to form modified Talc@TiO_2 composite particles.

To obtain visual information about the effect of an organic modifier on the dispersion of Talc@TiO_2, Fig. 5 shows photographs of modified Talc@TiO_2 in anhydrous ethanol for 10 min, 1 hour and 24 hours. All the surface modifiers have improved the dispersion of Talc@TiO_2 in organic solution. As time goes on, the NDZ201-Talc@TiO_2 solution has remained nearly unchanged and hardly formed any sediment throughout the entire process, suggesting that NDZ201 modified Talc@TiO_2 has the best dispersion and stability in organic solution. Their dispersion and stability increase in the following sequence: KH550-Talc@TiO_2 < PAAS-Talc@TiO_2 < NDZ201-Talc@TiO_2. Of great significance is that organic modification of Talc@TiO_2 greatly improves its compatibility with polymers to achieve the desired performance.

Fig. 6 shows the SEM images of organic modified Talc@TiO_2, with Talc@TiO_2 as a comparison, and their topography and structure under high magnifications are remarkably different. Talc@TiO_2 shows a low modification density of TiO_2 nanoparticles and poor dispersion with some aggregates. A micrograph of KH550-Talc@TiO_2 illustrates that KH550 modified TiO_2 nanoparticles with good dispersion have adhered to the surface of Talc and formed mixed particles with local aggregation. An SEM image of PAAS-Talc@TiO_2 shows that ACUMER9300 modified TiO_2 particles are unevenly dispersed in

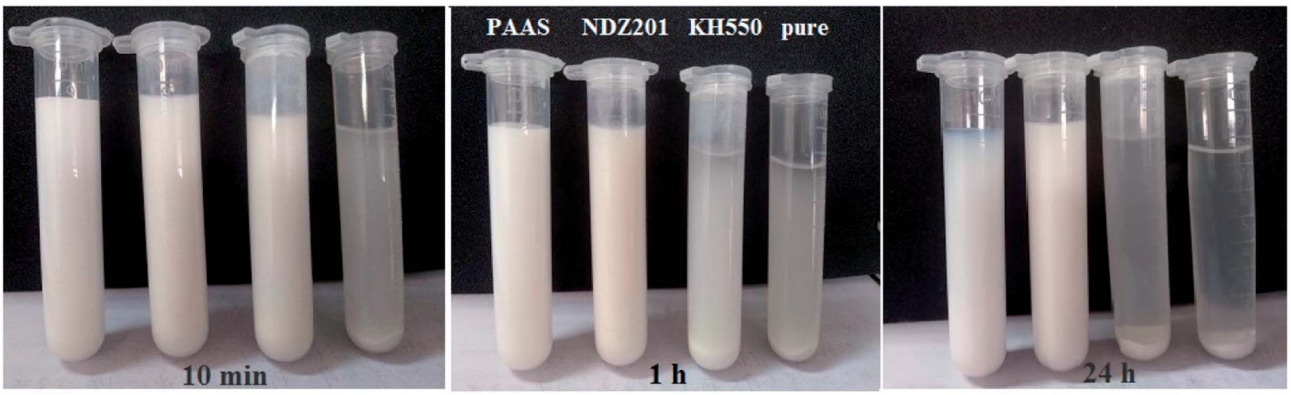

Fig. 5 Sedimentation of Talc@TiO_2 and modified Talc@TiO_2 (including PAAS-Talc@TiO_2, NDZ201-Talc@TiO_2, KH550-Talc@TiO_2) in anhydrous ethanol for 10 min, 1 hour and 24 hours.

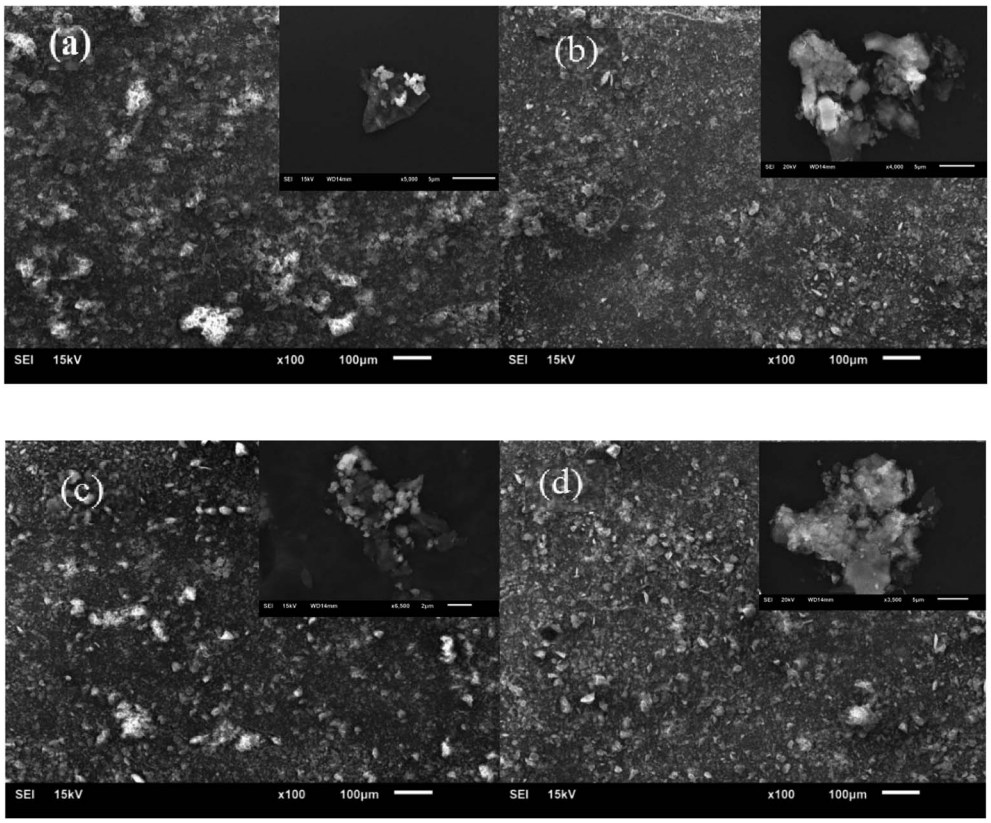

Fig. 6 SEM images of (a) Talc@TiO_2, (b) NDZ201-Talc@TiO_2, (c) KH550-Talc@TiO_2, (d) PAAS-Talc@TiO_2.

Talc and there are relatively large aggregates. NDZ201-Talc@TiO_2 displays a relatively regular shape, uniform size, and good dispersion morphology. The results illustrate that organic modified TiO_2 particles are more inclined to form a mixed structure *via* effectively adhering to the surface of Talc, especially coupling agents. The agglomeration of raw TiO_2 nanoparticles is easily caused in the process of preparation, but organic modified ones have good dispersion and hold a better prospect of application.

To verify the functional groups of organic modified Talc@TiO_2, FTIR was used to obtain the characteristic absorption peaks of the samples. Fig. 7 shows the FTIR spectra of all the specimens. The peaks at 788 cm^{-1} and 872 cm^{-1} are assigned to the Si–O–Si stretching band and Si–C stretching band, respectively.[41] The peak at around 1637 cm^{-1} is the OH bending vibration of the adsorbed and interlayer of TiO_2. Compared with Talc@TiO_2, modified Talc@TiO_2 particles have peaks nearby at 2850 cm^{-1} and 2920 cm^{-1}, which are assigned to the CH_3 symmetric stretching vibration of saturated alkyl and CH_2 antisymmetric stretching vibration of long chain alkyl.[42] The characteristic peak at 1442 cm^{-1} is due to the bending vibration mode of the carboxyl groups. For KH550-Talc@TiO_2, a sharper Si–O vibration peak at 1017 cm^{-1} reveals the exposure of the organic functional groups on Talc@TiO_2.[41] Peaks at 1317 cm^{-1} and 1382 cm^{-1} are attributed to the appearance of COO–, indicating that PAAS has been absorbed on the surface of Talc@TiO_2.

To further explore the modification mechanism, XPS was used to confirm the chemical states of the typical elements. XPS spectra of the samples are shown in Fig. 8. Talc@TiO_2 gives the $Ti2p_{1/2}$ peak at 464.7 eV and the $Ti2p_{3/2}$ peak at 459.4 eV, which are attributed to TiO_2. NDZ201-Talc@TiO_2 gives the $Ti2p_{1/2}$ peak at 464.7 eV and the $Ti2p_{3/2}$ peak at 459.1 eV, $Ti2p_{3/2}$ peak has undergone chemical shift due to the change in valence state from Ti^{4+} to Ti^{2+} and their alteration.[43] Compared with Talc@TiO_2, the Si2p peaks of KH550-Talc@TiO_2 have moved to a higher binding energy and a new peak is located at 103.4 eV, which is due to triethoxy silane,[44] illustrating that the silane coupling agent has adhered to the surface/interface of Talc@TiO_2 to achieve good dispersion and compatibility in the matrix materials. As can be seen in Fig. 8e, the XPS spectrum of original Talc@TiO_2 offers low binding energy C1s peaks at 284.6 eV, 285.0 eV and 285.6 eV, which are mainly attributed to carbon and its compounds from the surrounding environment. The XPS spectrum of PAAS-Talc@TiO_2 in Fig. 8f shows C1s peaks with higher binding energies, located at the binding energies of 288.9 eV, 286.7 eV and 285.4 eV, which are assigned to C═O, C–O and the alkyl chain from PAAS, respectively,[45] thereby indicating the existence of PAAS on the Talc@TiO_2 particles *via* physical adsorption and the chemical interaction between functional groups and the hydroxyl or carbonyl groups of nano-TiO_2.

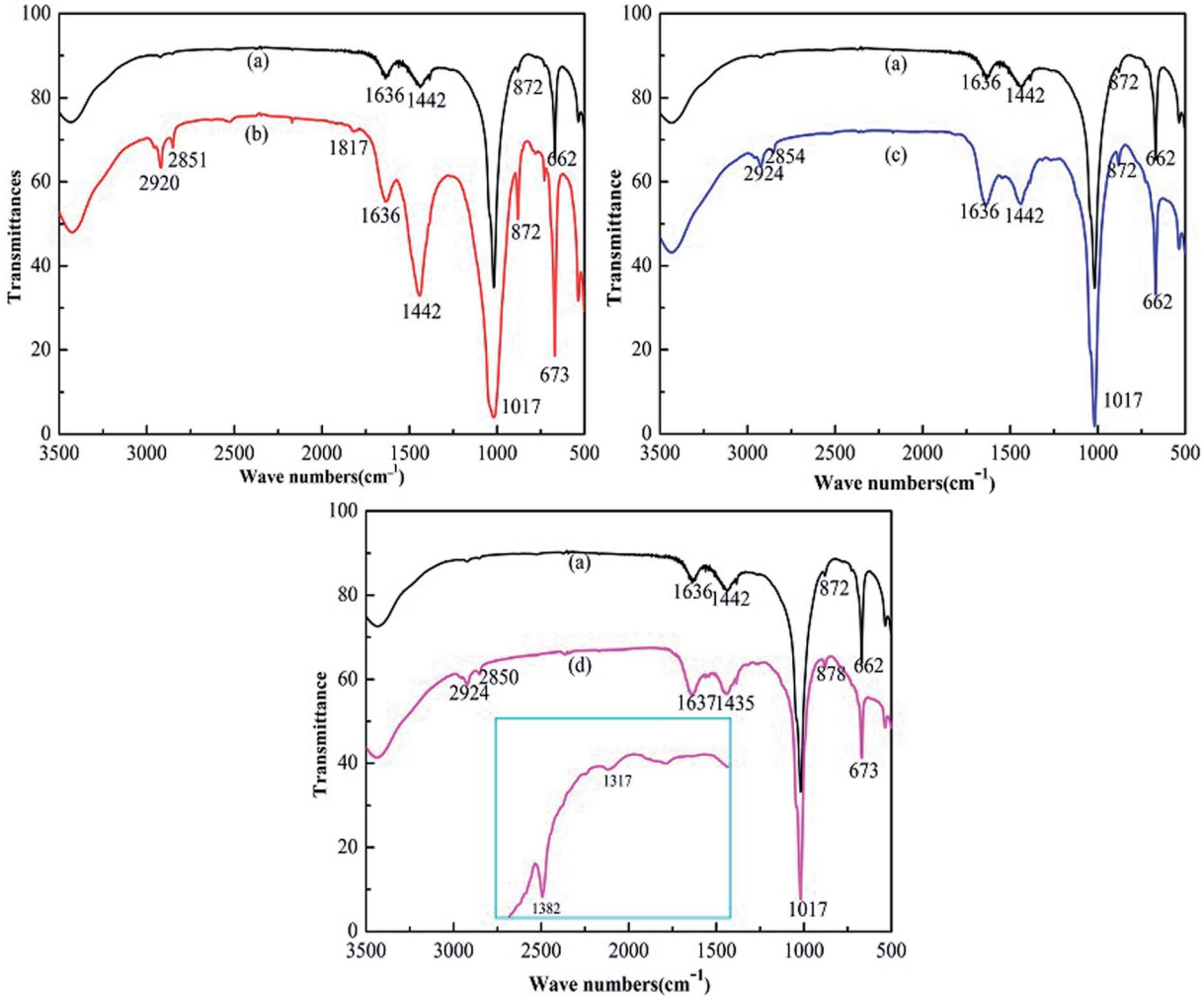

Fig. 7 FTIR spectra of (a) Talc@TiO_2, (b) NDZ201-Talc@TiO_2, (c) KH550-Talc@TiO_2, (d) PAAS-Talc@TiO_2.

3.3 Performance characteristics of modified Talc@TiO_2 hybrid XNBR

3.3.1 Mechanical properties. Fig. 9 shows that these modified Talc@TiO_2 fillers can increase the tensile strength of XNBR. The tensile strength has been improved by nearly 140% from 1.31 MPa to 3.10 MPa. In particular, XNBR with KH550-Talc@TiO_2 was not easily broken, and PAAS-Talc@TiO_2 also effectively strengthens the matrix. The addition of modified fillers can strengthen the interface effect with the matrix. Fillers with good dispersity exert a better adhesion between the fillers and the matrix, thereby enhancing the toughness of the XNBR.[46,47]

3.3.2 Dynamic mechanical analysis. To investigate the effect of Talc@TiO_2 as a filler on the performance of XNBR, Fig. 10 first gives the effect of filler content on the storage modulus and tan δ of XNBR. The storage modulus increases with an increase in amount of filler added, but the change in tan δ is inconsistent with the storage modulus. The tan δ value is close to 1.1, and 10 wt% Talc@TiO_2 as filler in XNBR gives the highest value. Therefore, XNBR with 10 wt% modified Talc@TiO_2 filler will be investigated in detail in the following.

Fig. 11 shows the dynamic mechanical analysis data of modified Talc@TiO_2 hybrid XNBR, including the storage modulus and tan δ. The storage modulus of modified Talc@TiO_2 hybrid XNBR reduces gradually with an increase in temperature, but they display a higher storage modulus at low temperature. Their tan δ values are generally consistent with that of original Talc@TiO_2 hybrid XNBR, and all of them are close to about 1.1, because the Talc@TiO_2 filler has the same basic composition, namely the same matrix material. The increase in storage modulus at lower temperature indicates that organic modification improves the compatibility and adhesion between the filler and XNBR, and modified Talc@TiO_2 as a filler can strengthen the elasticity of XNBR.[48]

3.3.3 Analysis of impact wear test. The initial velocity of the impact block was nearly 120 mm s^{-1} and its mass was 198.0 g. Fig. 12 shows the impact testing data. The impact force can reflect the elasticity of the filler hybrid XNBR: namely, a higher impact force means higher elasticity. Compared with Talc@TiO_2 hybrid XNBR, modified Talc@TiO_2 as a filler obviously enhances the impact force between the impact block and the XNBR matrix material, because organic modification of

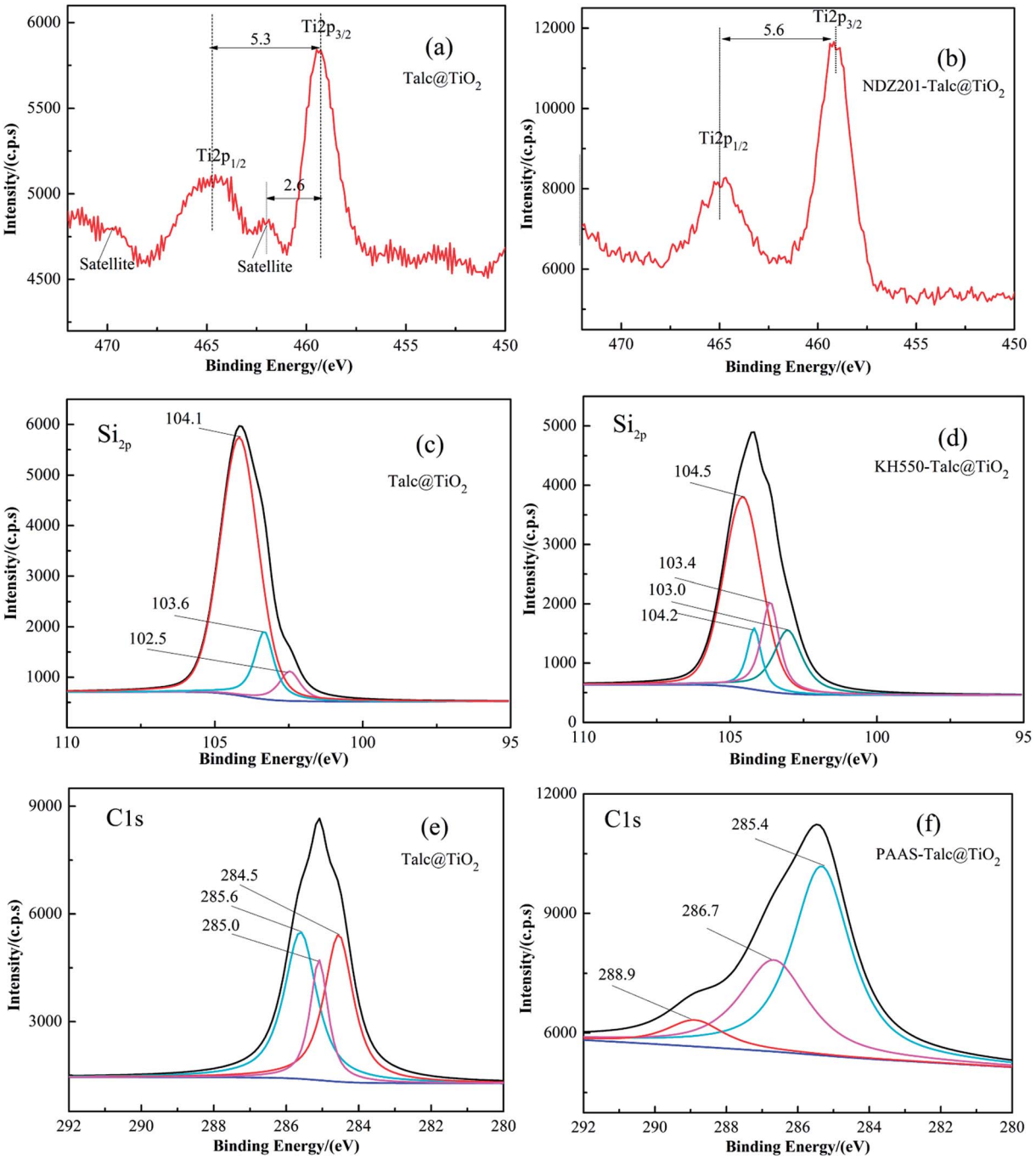

Fig. 8 XPS spectra, the fitting of Si2p and C1s peaks of original and modified Talc@TiO_2 by approximating the contribution of the background by the Shirley method.

Talc@TiO_2 improves the compatibility and adhesion with XNBR, and modified Talc@TiO_2 plays a larger role in the mechanical performance of the matrix material. The kinetic energy was calculated from $mv^2/2$, and the initial kinetic energy was 1.425 mJ. As filler hybrid XNBR suffers from an impact force, the kinetic energy tends to reduce due to the cushioning effect of the elastomer. They absorb energy and the corresponding rates are shown in Fig. 11c. The effect of modified Talc@TiO_2 on the performance of XNBR increases as follows: NDZ201 < KH550 < PAAS. The results illustrate that PAAS as an organic modifier not only improves the dispersion and compatibility of Talc@TiO_2 in XNBR, but also enhances the viscoelasticity of XNBR through adjusting the structure and thickening effect.

3.3.4 Morphology analysis of modified Talc@TiO_2 hybrid XNBR. To verify the filling performance of modified Talc@TiO_2 as fillers in XNBR, SEM was used to obtain cross-sectional micrograms. Fig. 13 show the cross-sectional images of

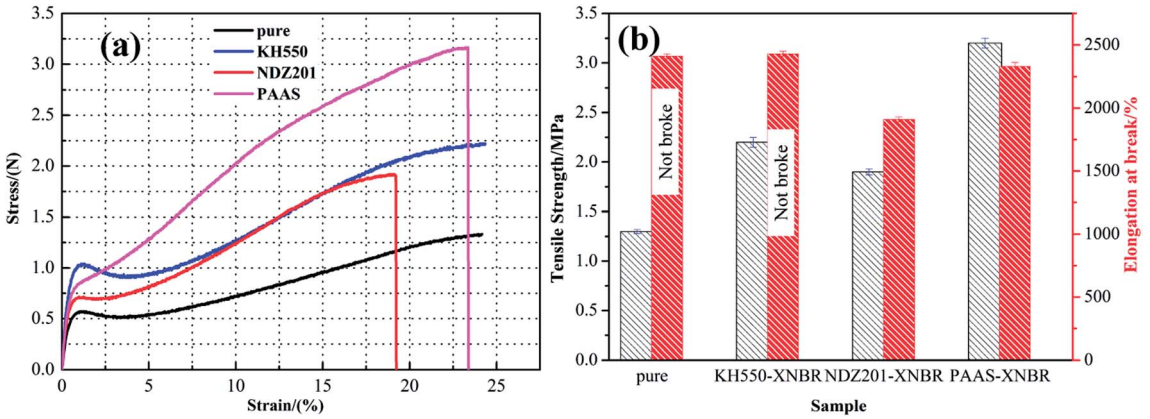

Fig. 9 Mechanical properties of XNBR with 15 wt% fillers: (a) stress–strain curves, (b) tensile strength and elongation at break.

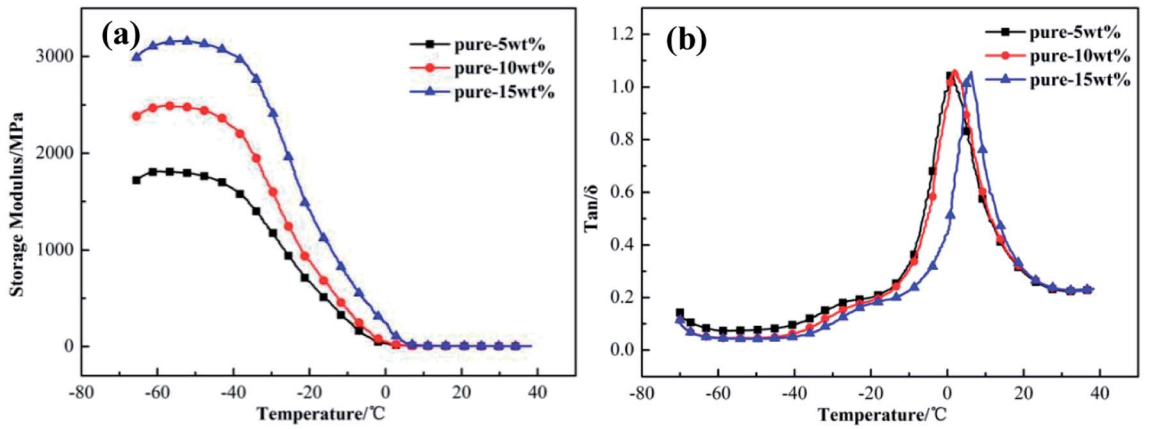

Fig. 10 Storage modulus (a) and tan δ (b) of Talc@TiO_2 as a filler in XNBR.

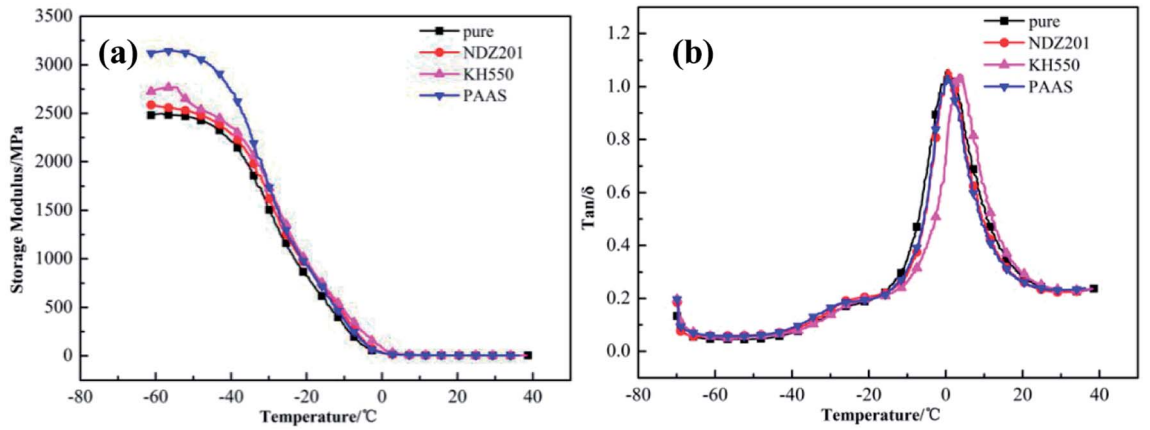

Fig. 11 Storage modulus (a) and tan δ (b) of modified Talc@TiO_2 as a filler in XNBR, with original Talc@TiO_2 as a comparison.

modified Talc@TiO_2 hybrid XNBR, which proves the intuitive differences between these fillers in XNBR. Talc@TiO_2 hybrid XNBR presents lots of irregular wrinkles, mainly due to poor adhesion and ductile fracture. PAAS modified Talc@TiO_2 particles were well distributed in XNBR and showed a relatively smooth cross section with few modified or coated particles, which seems to be consistent with the matrix material, so the excellent mechanical properties of PAAS-Talc@TiO_2 hybrid XNBR can be attributed to the effect of the organic modifier and good adhesion. The cross section of KH550-Talc@TiO_2 hybrid

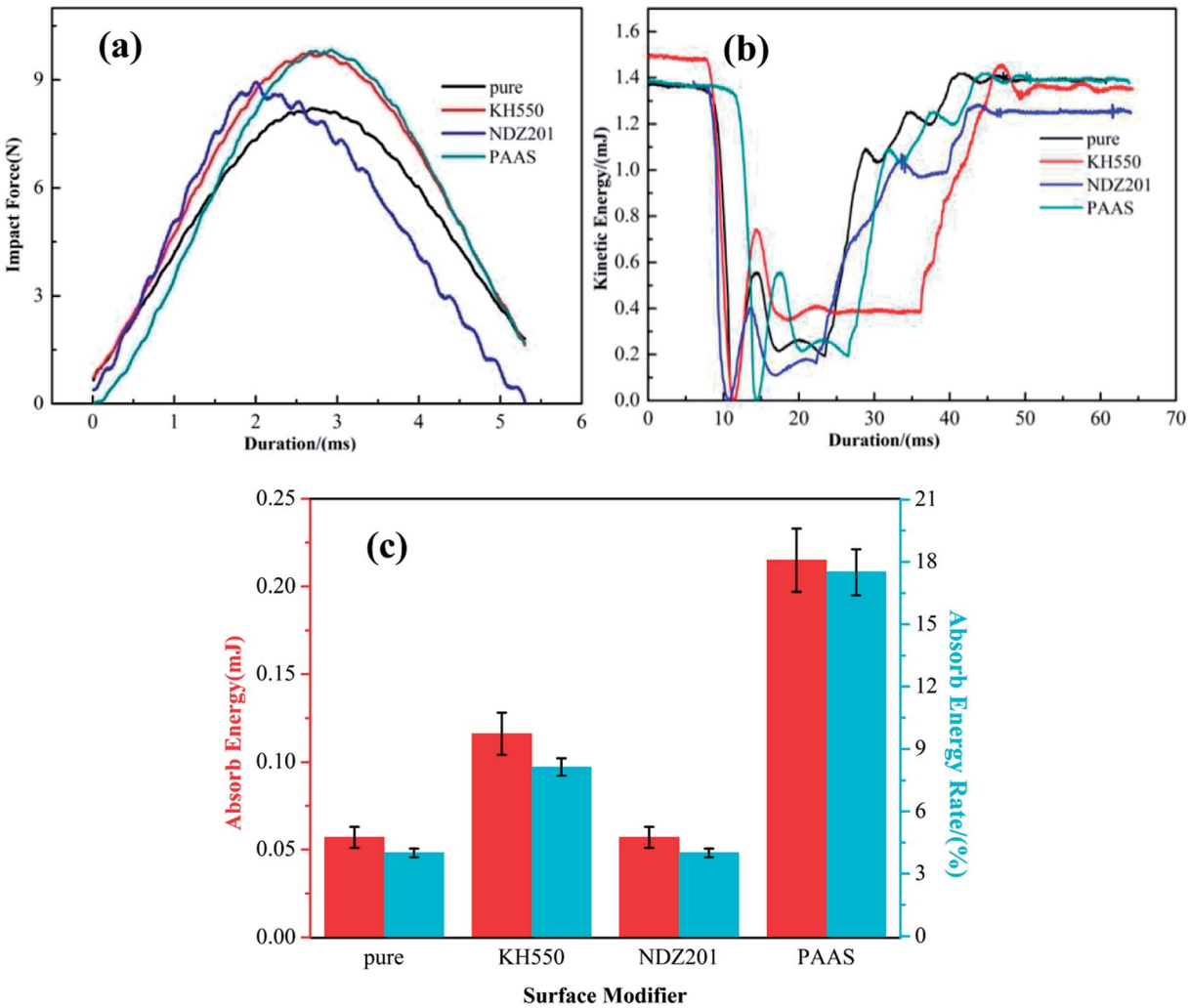

Fig. 12 Impact force (a), kinetic energy (b), absorbance of energy and the corresponding rate (c) of XNBR with the modified fillers.

XNBR shows some particles of different sizes, suggesting that KH550 modified Talc@TiO_2 cannot be well dispersed in XNBR, which is consistent with the results on the analysis of modified Talc@TiO_2. XNBR with NDZ201-Talc@TiO_2 as filler shows a different cross section with some small-size particles, so its elasticity could be reduced by the introduction of NDZ201. The results illustrate that PAAS plays an active role in the modification of inorganic filler and performance improvement of XNBR. The introduction of NDZ201 provides a higher dispersion of Talc@TiO_2 rather than enhancing the mechanical properties of XNBR. These performances depend mainly on high-density modification, good adhesion, and the nature of the modifier and filler.

Combined with the analysis of modified Talc@TiO_2 and hybrid XNBR, PAAS is the best choice as modifier according to the modification effect and performance characteristics of hybrid XNBR. By contrast, PAAS-Talc@TiO_2 hybrid XNBR possesses excellent performances including good adhesion, a high storage modulus and absorbance of energy, depending mainly on the good compatibility and thickening effect of the modifier. For KH550-Talc@TiO_2 hybrid XNBR, as KH550 modified Talc@TiO_2 was introduced into XNBR, XNBR and KH550 modifier interacted to form KH550-coupled XNBR with modified Talc@TiO_2, so this also illustrates that KH550 can offer relatively favorable mechanical properties.

4. Conclusions

Three modified Talc@TiO_2 particles were successfully prepared and were introduced into XNBR to investigate their compatibility and mechanical performance, such as damping capacity and impact resistance. The following conclusions can be reached:

(a) Talc@TiO_2 mixed particles were prepared *via* the ball-milling treatment of coupling agents and surfactant modified TiO_2 nanoparticles and Talc. NDZ201-Talc@TiO_2 particles show hydrophobicity, and PAAS-Talc@TiO_2 has good dispersion and compatibility in nitrile rubber.

(b) PAAS modified Talc@TiO_2 particles hybrid XNBR shows better adhesion and good damping capacity and impact resistance, which is attributed to the excellent mechanical property

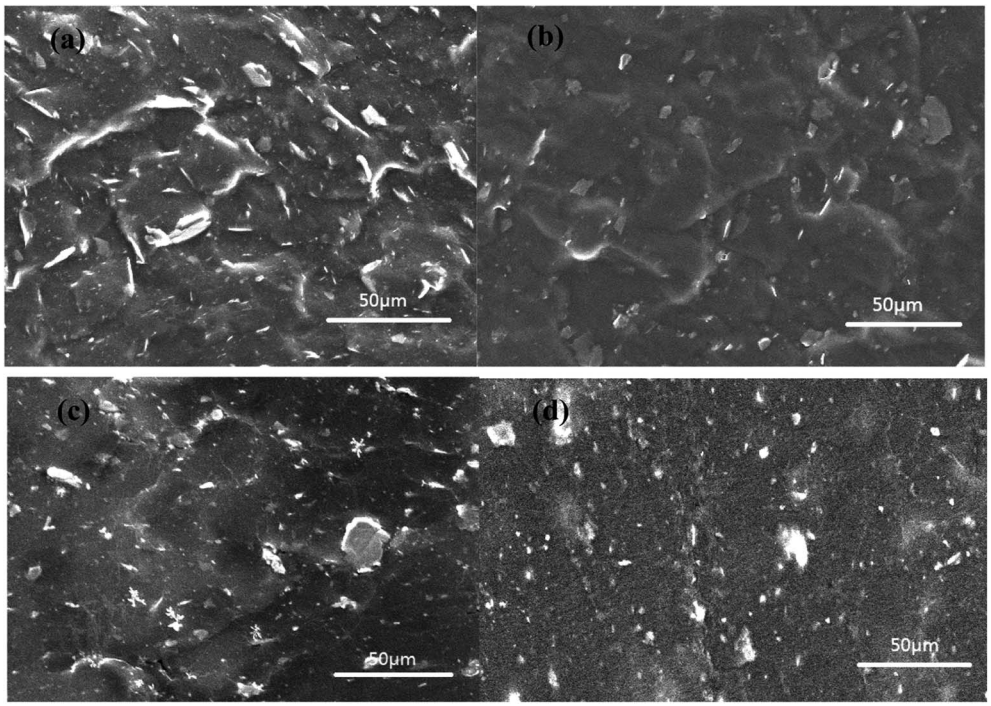

Fig. 13 Cross-sectional SEM images of XNBR with original Talc@TiO_2 (a) and modified Talc@TiO_2 by (b) PAAS, (c) KH550, (d) NDZ201.

of Talc, good adhesion between modified Talc@TiO_2 and XNBR, and the nature of PAAS.

(c) The enhancement effect of modified Talc in XNBR was investigated in detail, and organic modification of Talc offers a great deal of flexibility. It is hoped that high-density modified Talc@TiO_2 or organic clay as fillers can offer a significant step toward real-world application for polymers.

Conflicts of interest

There are no conflicts to declare.

Acknowledgements

The authors gratefully acknowledge the financial support provided by the National Natural Science Foundation of China (No. 51705435 and No. 51627806), the Changjiang Scholarships and Innovation Team Development Plan (No. IRT1178).

References

1 H. Kargarzadeh, M. Mariano, J. Huang, N. Lin, I. Ahmad, A. Dufresne and S. Thomas, *Polymer*, 2017, **132**, 368–393.
2 B. Likozar and Z. Major, *Appl. Surf. Sci.*, 2010, **257**, 565–573.
3 B. Chen, J. R. G. Evans, H. C. Greenwell, P. Boulet, P. V. Coveney, A. A. Bowden and A. Whiting, *Chem. Soc. Rev.*, 2008, **37**, 568–594.
4 N. D. Bansod, B. P. Kapgate, C. Das, D. Basu, S. C. Debnath, K. Roy and S. Wiessner, *RSC Adv.*, 2015, **5**, 53559–53568.
5 H. Kursun and U. Ulusoy, *Int. J. Miner. Process.*, 2006, **78**, 262–268.
6 S. DíEz-Gutiérrez, M. A. RodríGuez-Pérez, J. A. D. Saja and J. I. Velasco, *Polymer*, 1999, **40**, 5345–5353.
7 J. C. Dai and J. T. Huang, *Appl. Clay Sci.*, 1999, **15**, 51–65.
8 Y. P. Wu, Q. X. Jia, D. S. Yu and L. M. Zhang, *J. Appl. Polym. Sci.*, 2010, **89**, 3855–3858.
9 A. Krysztafkiewicz and L. Domka, *J. Mater. Chem.*, 1997, **7**, 1655–1659.
10 W. J. Choi and S. C. Kim, *Polymer*, 2004, **45**, 2393–2401.
11 B. Fiorentino, R. Fulchiron, J. Duchet-Rumeau, V. Bounor-Legaré and J. C. Majesté, *Polymer*, 2013, **54**, 2764–2775.
12 K. P. Sau, T. K. Chaki and D. Khastgir, *J. Mater. Sci.*, 1997, **32**, 5717–5724.
13 Y. Shangguan, J. Yang and Q. Zheng, *RSC Adv.*, 2017, **7**, 15978–15985.
14 E. G. Bajsic, F. Veljko and V. O. Bulatovc, *Adv. Mater. Res.*, 2014, **849**, 121–126.
15 Y. Jahani and M. Ehsani, *Polym. Bull.*, 2009, **63**, 743–754.
16 N. Petchwattana, S. Covavisaruch and S. Petthai, *Polym. Bull.*, 2014, **71**, 1947–1959.
17 A. Garnier, F. Da Cruz-Boisson, S. Rigolet, J. Brendlé and V. Bounor-Legaré, *RSC Adv.*, 2016, **6**, 75715–75723.
18 L. A. Castillo, S. E. Barbosa, P. Maiza and N. J. Capiati, *J. Mater. Sci.*, 2011, **46**, 2578–2586.
19 A. Krysztafkiewicz, L. Domka and W. Wieczorek, *Colloid Polym. Sci.*, 1985, **263**, 804–811.
20 J. Zhang, H. Zhang, J. Pang, L. Li, S. Wang and M. Liu, *RSC Adv.*, 2016, **6**, 104416–104424.
21 L. Zang, D. Chen, Z. Cai, J. Peng and M. Zhu, *Composites, Part B*, 2018, **137**, 217–224.
22 Q. Y. Fan and H. B. Zhan, *Prog. Chem.*, 2012, **24**, 54–60.
23 Z. Zhang, X. He, J. Zhang, X. Lu, C. Yang, T. Liu, X. Wang and R. Zhang, *RSC Adv.*, 2016, **6**, 91798–91805.

24 S. Kango, S. Kalia, A. Celli, J. Njuguna, Y. Habibi and R. Kumara, *Prog. Polym. Sci.*, 2013, **38**, 1232–1261.
25 H. H. Huang, A. H. Sun, J. F. Zhang, B. Wang, C. Y. Chu, Y. Li and G. J. Xu, *Mater. Lett.*, 2013, **110**, 260–263.
26 S. Ullah, E. P. Ferreira-Neto, A. A. Pasa, C. C. J. Alcantara, J. J. S. Acuña, S. A. Bilmes, M. L. M. Ricci, R. Landers, T. Z. Fermino and U. P. Rodrigues-Filho, *Appl. Catal., B*, 2015, **179**, 333–343.
27 C. Ocando, A. Tercjak and I. Mondragon, *Eur. Polym. J.*, 2011, **47**, 1240–1249.
28 S. C. Tjong, *Mater. Sci. Eng., R*, 2006, **53**, 73–197.
29 D. F. Schmidt and E. P. Giannelis, *Chem. Mater.*, 2010, **22**, 167–174.
30 G. Cheng, B. Tong, Z. F. Tang, X. H. Yu, H. L. Wang and G. X. Ding, *Appl. Surf. Sci.*, 2014, **313**, 954–960.
31 Z. Demjen, B. Pukánszky, E. Földes and J. Nagy, *J. Colloid Interface Sci.*, 1997, **190**, 427–436.
32 J. Z. Lu, Q. L. Wu and H. S. J. Mcnabb, *Wood Fiber Sci.*, 2000, **32**, 88–104.
33 P. C. Ma, J. Kim and B. Z. Tang, *Carbon*, 2006, **44**, 3232–3238.
34 P. Yang and M. G. Moloney, *RSC Adv.*, 2016, **6**, 111276–111290.
35 A. Vermogen, K. Masenelli-Varlot and R. Séguéla, *Macromolecules*, 2005, **38**, 9661–9669.
36 S. Pradhan, F. R. Costa, U. Wagenknecht, D. Jehnichen, A. K. Bhowmick and G. Heinrich, *Eur. Polym. J.*, 2008, **44**, 3122–3132.
37 H. L. Kang, K. H. Zuo, Z. Wang, L. Q. Zhang, L. Liu and B. C. Guo, *Compos. Sci. Technol.*, 2014, **92**, 1–8.
38 K. Sasikumar, N. R. Manoj, T. Mukundan and D. Khastgir, *Composites, Part B*, 2016, **92**, 74–83.
39 Spectral Database for Organic Compounds. SDBS, http://sdbs.db.aist.go.jp/sdbs/cgi-bin/direct_frame_top.cgi.
40 D. M. Zhang, H. L. Yang, S. W. Yu and X. M. Sang, *Key Eng. Mater.*, 2008, **368**, 1477–1479.
41 J. R. Sohn and H. J. Jang, *J. Catal.*, 1991, **132**, 563–565.
42 S. Yoon, R. J. Holiday, E. L. Sibert and F. F. Crim, *J. Chem. Phys.*, 2003, **119**, 9568–9575.
43 NIST X-ray Photoelectron Spectroscopy Database, National Institute of Standards and Technology: Gaithersburg. http://srdata.nist.gov/xps/.
44 E. T. Vandenberg, L. Bertilsson, L. Bo, K. Uvdal, R. Erlandsson, H. Elwing and I. Lundström, *J. Colloid Interface Sci.*, 1991, **147**, 103–118.
45 X. Wallart, C. H. D. Villeneuve and P. Allongue, *J. Am. Chem. Soc.*, 2005, **127**, 7871–7878.
46 J. Y. Wang, H. B. Jia, Y. Y. Tang, D. D. Ji, Y. Sun, X. D. Gong and L. F. Ding, *J. Mater. Sci.*, 2013, **48**, 1571–1577.
47 I. Smaoui, A. Domatti, M. Kharrat, M. Dammak and G. Monteil, *Fullerenes, Nanotubes, Carbon Nanostruct.*, 2017, **24**, 769–778.
48 A. K. Mehrjerdi, B. Adl-Zarrabi, S. W. Cho and M. Skrifvars, *J. Appl. Polym. Sci.*, 2013, **129**, 2128–2138.